

Variable Diagonal Loading Based Robust Concentric Hexagonal Antenna Array with Low Side Lobe Level Using Tapering Windows

Md. Y. Ali*, Md. S. Hossain, and Md. F. Reza

Abstract—In this paper, the performance of a concentric hexagonal antenna array (CHAA) is investigated with the exploitation of a robust variable diagonal loading (VDL) technique in the presence of direction of arrival (DOA) mismatch. The performance of minimum variance distortionless response (MVDR) based CHAA is compared with the performance of existing MVDR based concentric circular antenna arrays (CCAAs), and it is found that the proposed MVDR based CHAA provides 25.54% narrow half-power beamwidth (HPBW) and lower side lobe level than the existing MVDR based CCAA. When DOA mismatch occurs between main beam steering direction and actual signal-of-interest (SOI) direction, the performance of MVDR based CHAA is deteriorated. In the case of DOA mismatch, to ameliorate the performance of CHAA, this paper proposes VDL technique for the CHAA processor and compares the performance of the proposed robust CHAA with the existing robust CHAAs. The proposed VDL based robust CHAA delivers 88.37% and 78.56% higher output power for 2° DOA mismatch than existing fixed diagonal loading (FDL) and optimal diagonal loading (ODL) based CHAAs, respectively. Several tapering window functions are proposed to reduce the side lobe level of CHAA. Performance of the proposed beamformer is analyzed utilizing MATLAB environment in various scenarios.

1. INTRODUCTION

Many applications like radio astronomy, radar, sonar, wireless communication, satellite communications, and imaging where such type of radiation properties is needed cannot be achieved using single antenna. Smart antenna arrays are widely used in these types of applications due to their adaptive characteristics and lots of advantages like system capacity enhancement, energy efficiency, and smart management to fulfill their certain radiation characteristics [1]. Smart antennas work based on the principle of beamforming. The process to aggregate the weighted signals after multiplying with required weight of individual antenna elements to produce a beam of electromagnetic energy to any desired direction rather than in all directions is known as beamforming [2]. The radiation pattern of a smart antenna can be shaped with different structures of the overall array [3].

Linear [4, 5] and circular [6, 7] structures are used for smart antennas. Linear antenna array produces the narrowest beamwidth and higher directivity, but the shortcoming of this array is that it cannot scan over 360° azimuth angle, and the dimension of linear antenna array becomes large when a large number of antenna elements are incorporated in this array. Circular and hexagonal antenna arrays have the capability to scan signal over 360°. It is desired to obtain high gain, high directivity, higher interference rejection capability, lower SLL, and more robustness in the appearance of DOA error, but very few antenna arrays in the previous literature have the capability to provide the desired performances simultaneously.

Received 6 June 2020, Accepted 9 July 2020, Scheduled 21 July 2020

* Corresponding author: Md. Yeakub Ali (yeakub.ruet08@gmail.com).

The authors are with the Department of Electrical and Electronic Engineering, Rajshahi University of Engineering & Technology, Rajshahi, Bangladesh.

Conventional antenna array also known as delay-and-sum antenna array is incapable to cancel any kind of directional interference whereas MVDR beamformer is able to reject the directional interference. The performance of MVDR beamformer deteriorates when DOA error appears between estimated SOI direction and actual SOI direction. There are some approaches to mitigate the problem of MVDR beamformer in the appearance of DOA mismatch. Diagonal loading (DL) technique is a notable one discussed in [8–13]. ODL [14] and VDL [7, 15] techniques have been applied on CCAA to make the array system robust whose performance is better than a linear antenna array. ODL robust technique has been exploited in hexagonal antenna array in [16]. Circular array has been compared with hexagonal antenna array using different optimization techniques in [17, 18]. Adaptive techniques can be utilized associated with robust techniques for smart antenna array discussed in [19–24].

There are a few approaches for side lobe level (SLL) reduction of power pattern. Optimization techniques like cat swarm optimization [5, 6] and particle swarm optimization [25, 26] are utilized for SLL reduction. Tapering with different windows is also exploited to lessen SLL discussed in [27–29]. In this paper, tapering windows are exploited to reduce the SLL of CHAA and analyze the performance. Experimental analysis with an antenna prototype of planner and circular polarized dipole antenna array for wireless communication is shown in [30–32]. So we can say that it is feasible to implement our proposed CHAA in practical application.

To increase the directivity and gain of an array in any desired direction and techniques to suppress any interference still attract great interest. The aim of this paper is to enhance the directivity and robustness in appearance of DOA error and minimize SLL. In this paper, a CHAA using VDL technique is presented in the presence of DOA error which delivers better performance than the existing CHAAs [16] and CCAA [14]. Moreover, some conventional window functions have been modified and applied to CHAA to taper the SLL. Characteristics of the proposed CHAA are as follows:

- Deliver better performance than existing CHAAs [16] and CCAA [7] beamformer.
- Have capability of steering the beam in any intended direction.
- Be Efficient to nullify directional interference and more robust in appearance of DOA error.
- Produce lower SLL using tapering windows.

The remainder of this paper is organized as follows. In Section 2, system model and array geometry are depicted. Different types of beamforming techniques and various tapering windows for CHAA are described in Sections 3 and 4, respectively. In Section 5, simulation results are discussed, and the performance of the proposed CHAA beamformer is evaluated. Section 6 draws the conclusion.

2. SYSTEM MODEL AND ARRAY GEOMETRY

A hexagonal antenna array based narrowband communication system is shown in Fig. 1. The induced signals on the elements are multiplied by required weights and then summed up for output signal of the system. The information of output signal and SOI direction are provided to array processor to estimate the weights. The geometry of the CHAA is portrayed in Fig. 2. The CHAA structure may consist of n elements in one side of the structure. Here, $n = 2, 3, 4, \dots, M$, and M is the required maximum number of elements in one side which depends on the required application and other required performance parameters. The distance between two elements is d which should be half wavelength for optimum performance, and all elements are equally distant. There is an element in the center of the hexagonal structure, and this structure is symmetric in the configuration. Because of the center element, the SLL is diminished compared to the structure without a center element.

If the number of elements in one side of the structure is n , the total number of rows of elements will be $2n - 1$. The total number of elements in the whole structure will be

$$\mathcal{N} = 2 \sum_{k=0}^{n-2} (n+k) + r \quad (1)$$

where \mathcal{N} is the total number of elements, and $r = 2n - 1$ is the total number of rows in the hexagonal structure. The radius of the structure is equal to $(n - 1) * d$. In Fig. 2, the plane wave-front of the incoming signal is incident on the array at azimuth angle φ and elevation angle θ . If the positions of

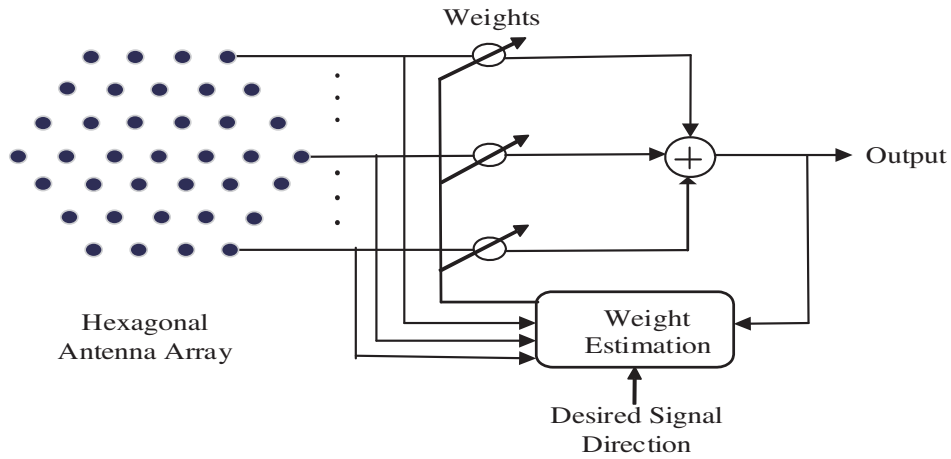


Figure 1. Block diagram of a CHAA based narrowband communication system.

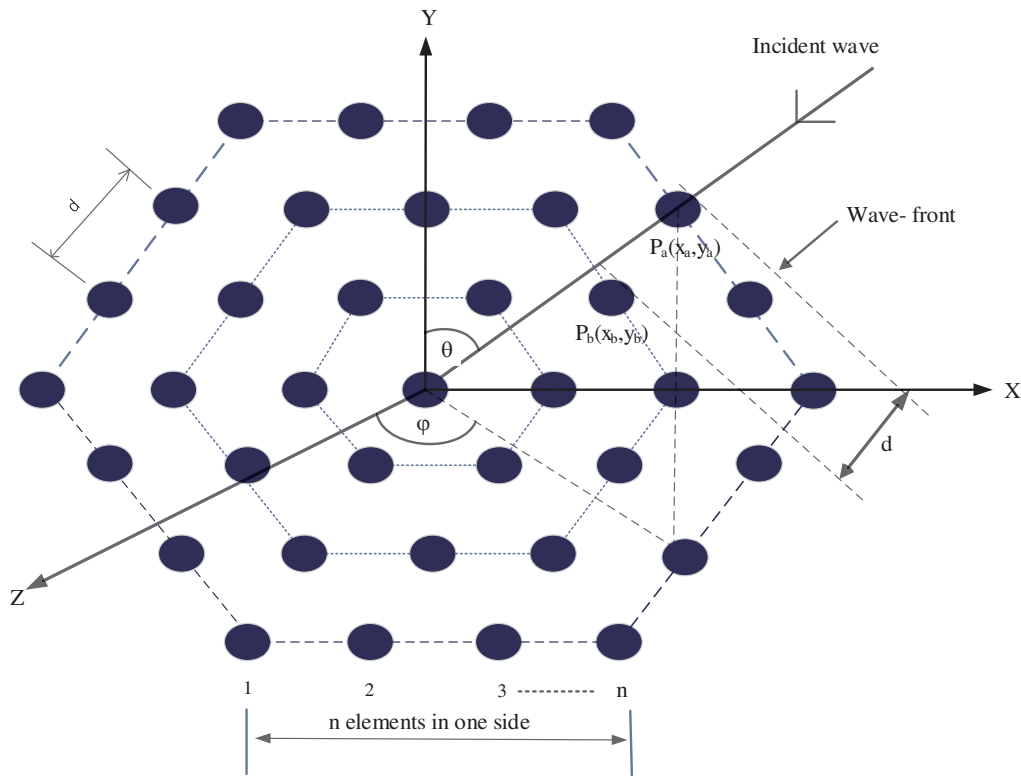


Figure 2. The geometry of the proposed CHAA beamformer.

two elements are indicated by P_a and P_b , the distance traveled by the wave-front from point P_a to P_b can be computed with axis rotation method as,

$$d = ((x_a - x_b) \cos \varphi + (y_a - y_b) \sin \varphi) * \cos \theta \tag{2}$$

Then, the time needed for the wave-front to propagate from point P_a to P_b is computed by,

$$\tau = \frac{d}{c} \tag{3}$$

where c denotes the velocity of incoming signal.

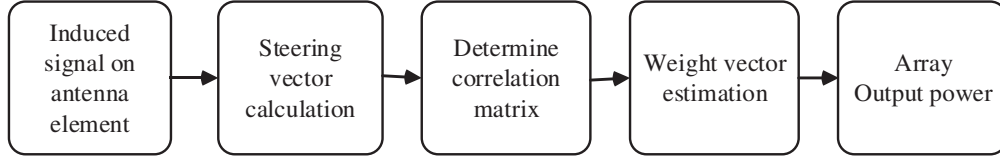


Figure 3. Steps to calculate array output power.

The step by step process to compute the output power of the beamformer is shown in Fig. 3. If $\mathbf{X}(t)$ represents received signal vector by the elements, and \mathbf{W} represents weight vector, the output of the system can be expressed as

$$\mathcal{O}(t) = \sum_{i=1}^L \mathbf{W}_i^* \mathbf{X}_i(t) \quad (4)$$

The output signal in vector notation becomes $\mathcal{O}(t) = \mathbf{W}^H \mathbf{X}(t)$, and output power is $\mathcal{P}(\mathbf{W}) = \mathbf{W}^H \mathcal{R} \mathbf{W}$, where $(\cdot)^T$ and $(\cdot)^H$ refer to transposition and complex conjugate transposition, respectively [2].

At any time the received signal by the reference element due to the k th source is $m_k(t) = e^{j2\Pi f_0 t}$, where $m_k(t)$ represents the modulating function, and f_0 represents the frequency of the carrier signal. If $\tau_l(\varphi_k, \theta_k)$ represents the delay from the l th element to the reference element, the received signal by the l th element due to the k th source is $m_k(t) = e^{j2\Pi f_0 (t + \tau_l(\varphi_k, \theta_k))}$. Due to M sources and system surrounding noise, the total induced signal on the l th element is given by [2],

$$\mathcal{X}_l(t) = \sum_{k=1}^M m_k(t) e^{j2\Pi f_0 (t + \tau_l(\varphi_k, \theta_k))} + n_l(t) \quad (5)$$

here, $n_l(t)$ is the noise received by the l th element. In this case, $E[m_k(t)n_l(t)] = 0$, which means that the noise is uncorrelated with SOI sources. The noise components received by the elements are also uncorrelated, which means $E[n_k(t)n_l(t)] = 0$ for $k \neq l$ and $E[n_k(t)n_l(t)] = \alpha_n^2$ for $k = l$, here, α_n^2 is the noise power. The correlation matrix considering the presence of noise and interference is expressed as [2],

$$\mathcal{R} = \mathcal{P}_d \mathbf{S}_d \mathbf{S}_d^H + \mathcal{P}_i \mathbf{S}_i \mathbf{S}_i^H + \alpha_n^2 \mathbf{I} \quad (6)$$

where \mathcal{P}_d , \mathcal{P}_i , \mathbf{S}_d , and \mathbf{S}_i denote SOI power, interference power, steering vector in steering direction, and steering vector in the interference direction, respectively.

3. BEAMFORMING TECHNIQUES

The performance of a beamformer is associated with the technique that is used for beamforming. Delay-and-sum and optimal are two major types of beamforming. Delay-and-sum antenna array is not capable to detect and reject interference. MVDR antenna array beamformer can trace the interference signal and nullify the signal. Robust techniques like FDL, ODL, and VDL are applied to ameliorate the performance of MVDR beamformer in appearance of DOA error. MVDR, FDL, ODL, and VDL techniques are described shortly in this section.

3.1. MVDR Beamforming

Delay-and-sum beamformers can produce limited output SNR as they require information about interference signal. MVDR beamformers can deliver maximum SNR if they have no DOA errors. MVDR based beamformer needs information of only SOI direction but does not need information about interference and noise signal to maximize SNR [9]. The array weight of this beamformer is mandatorily constrained to achieve unity response in the steering direction, that is,

$$\hat{\mathbf{W}}^H \mathbf{S}_d = 1 \quad (7)$$

The weight vector in MVDR based beamformer is

$$\hat{\mathbf{W}} = \frac{\mathcal{R}^{-1}\mathbf{S}_d}{\mathbf{S}_d^H \mathcal{R}^{-1}\mathbf{S}_d} \quad (8)$$

3.2. FDL Based Robust Beamforming

In the appearance of DOA mismatch, the MVDR beamformer considers the actual SOI as interference signal and nullify it. This performance degradation problem of MVDR beamformer against the DOA error can be mitigated using FDL robust technique. In FDL, to reduce the signal cancelation because of DOA error, a fixed value is added to the diagonal of the correlation matrix. Correlation matrix in FDL technique becomes [14],

$$\mathcal{R}_{FDL} = \mathcal{R}_{dis} + \gamma * \mathbf{I} \quad (9)$$

here, γ and \mathbf{I} indicate the diagonal loading factor and identity matrix, respectively. γ is commensurate to $10\alpha_n^2$, where α_n^2 is the surrounding noise. The challenge of choosing γ is discussed in [33].

3.3. ODL Based Robust Beamforming

Optimal diagonal loading (ODL) is one of the robust techniques which is used to enhance the robustness of beamformer in the appearance of DOA mismatch [14, 34]. Correlation matrix in ODL method considering DOA error is given by [14]

$$\mathcal{R}_{odl} = \mathcal{R}_{dis} + \gamma * \mathbf{I} \quad (10)$$

The value of γ is computed by

$$\gamma = \frac{\epsilon(\alpha_n^2 + \mathcal{P}_d \|\mathbf{S}_d\|^2)}{\|\mathbf{S}_{ac}\| - \epsilon} \quad (11)$$

where $\|\mathbf{S}_d\|$ and $\|\mathbf{S}_{ac}\|$ denote the norms of steering vector without and with DOA error. ϵ is known as steering vector distortion bound and computed by

$$\epsilon = \max(\|\mathbf{S}_d - \mathbf{S}_{ac}\|) \quad (12)$$

3.4. VDL Based Robust Beamforming

CHAA can be optimized for better performance using VDL technique than other techniques. The proposed CHAA exploiting VDL technique is self-acting, and the value of loading level relies on SOI power level, noise power level, norm of steering vector considering with DOA error and without DOA error, and steering vector distortion bound. Correlation matrix in VDL method because of DOA mismatch can be computed by [7],

$$\mathcal{R}_{VDL} = \mathcal{R}_{dis} + \mathcal{R}_{dis}^{-1} * \gamma * \mathbf{I} \quad (13)$$

The loading factor γ is calculated by the equation as follows

$$\gamma = \frac{\epsilon(\alpha_n^2 + \mathcal{P}_d \|\mathbf{S}_d\|^2)}{\|\mathbf{S}_{ac}\| - \epsilon} \quad (14)$$

where \mathcal{P}_d denotes the SOI power, α_n^2 the noise power, and $\|\mathbf{S}_d\|$ and $\|\mathbf{S}_{ac}\|$ denote the norms of steering vector not considering DOA error and considering DOA error, respectively. ϵ is computed as follows

$$\epsilon = \max(\|\mathbf{S}_d - \mathbf{S}_{ac}\|) \quad (15)$$

The increment of ϵ increases γ , and it approaches infinity when ϵ is equivalent to the norm of \mathbf{S}_{ac} . This VDL technique yields a close form expression for γ with little estimation and provides such a loading factor that has higher adaptation capability with look direction error than other techniques [11].

4. TAPERING WINDOWS FOR CHAA

The well recognized window functions like Uniform feeding, Triangular, Hamming, Hanning, Blackman, and Binomial windows in filtering application can be amended to utilize in CECHAA to minimize the SLL of the power pattern of CHAA discussed in [28]. The possibility to decrease the side lobe to main lobe ratio in the filter magnitude response is shown in [29]. In modified window function, the individual hexagonal ring is considered to be equivalent to an element of a linear array. So, the weights are identical of each element of a particular ring of CHAA. The coefficients of the rings for CHAA using different windows are described below where \mathcal{T} denotes the total ring, and m denotes the individual ring number.

Uniformly fed CHAA has the coefficients of equal amplitude for all the hexagonal rings, and the value of the coefficient is unity [28]. These coefficients yield lower beamwidth than other window schemes and maximum SLL. The coefficients can be expressed as

$$a_m = 1, \quad m = 1, 2, \dots, \mathcal{T} \quad (16)$$

The coefficients of triangular window follow a triangular function, and the amplitude of the coefficients of the rings for this window can be expressed as:

$$a_m = \frac{\mathcal{T} - m + 1}{\mathcal{T}}, \quad m = 1, 2, \dots, \mathcal{T} \quad (17)$$

where m is the ring number in the array. The coefficient for the center element is $a_1 = 1$, and the coefficient for the outermost ring is $a_m = 1/\mathcal{T}$.

The coefficients of the rings for a \mathcal{T} hexagonal ring CHAA system by using Hamming window can be amended as [35],

$$a_m = 0.54 - 0.46 \cos \left(\frac{\pi(\mathcal{T} - m - 2)}{\mathcal{T} + 1} \right), \quad m = 1, 2, \dots, \mathcal{T}. \quad (18)$$

The coefficients of the Hanning window [35] amended to suit for application in CHAA, which are similar to Hamming window, are expressed as

$$a_m = 0.5 - 0.5 \cos \left(\frac{\pi(\mathcal{T} - m - 2)}{\mathcal{T} + 1} \right), \quad m = 1, 2, \dots, \mathcal{T}. \quad (19)$$

The amended coefficients function for the CHAA using Blackman window can be expressed as

$$a_m = 0.42 - 0.5 \cos \left(\frac{\pi(\mathcal{T} - m - 2)}{\mathcal{T} + 1} \right) + 0.08 \cos \left(\frac{\pi(\mathcal{T} - m - 2)}{\mathcal{T} + 1} \right), \quad m = 1, 2, \dots, \mathcal{T} \quad (20)$$

In Binomial window the coefficient for CHAA can be expressed as [28],

$$a_m = \binom{2\mathcal{T} - 1}{\mathcal{T} + m - 1} \quad (21)$$

For the innermost ring $m = 1$, and for outermost ring $m = \mathcal{T}$.

5. PERFORMANCE ANALYSIS

Performance of the proposed CHAA has been analyzed and compared with an existing beamformer in this section. To analyze the performance, three and four elements in one side of the CHAA have been considered for different scenarios, respectively. For three elements in one side, the total number of elements is 19, and for four elements in one side, total number of elements is 37 in the array. Inter-element spacing, signal propagation speed, and signal frequency are half-wavelength, 3×10^8 m/s, and 0.3 GHz, respectively.

Figure 4 exhibits the power pattern comparison between the proposed MVDR based CHAA and MVDR based CCAA [7] with the same number of elements (19) where the beamwidth of CHAA is significantly narrower than the beamwidth of CCAA. For example, the HPBW of proposed CHAA and existing CCAA are 35.88° and 48.19° , respectively. So the HPBW of CHAA is 25.54% narrower than the HPBW of CCAA. The narrow beamwidth of CHAA raises the directivity and reduces the SLL

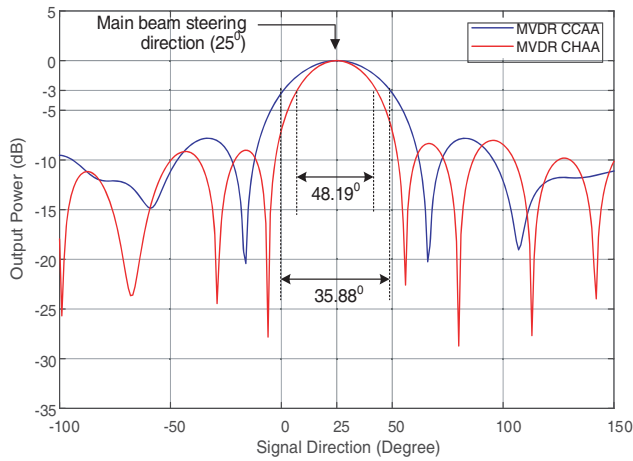


Figure 4. Beamwidth comparison between proposed MVDR based CHAA and existing MVDR based CCAA [7] with 19 elements for both beamformer.

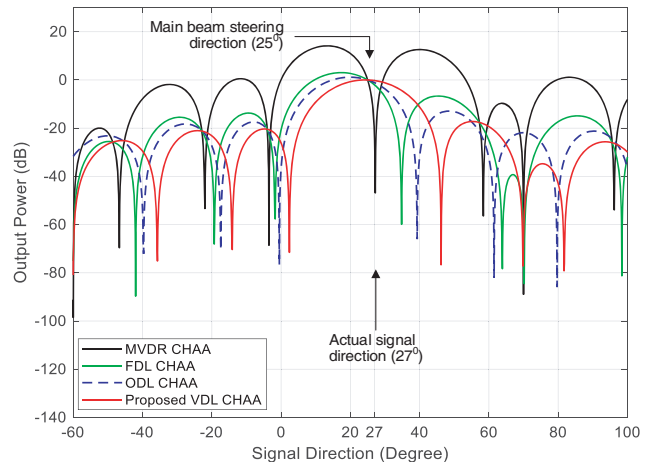


Figure 5. Power pattern comparison among MVDR, FDL, ODL [16] and proposed VDL based robust CHAA with 2° DOA error.

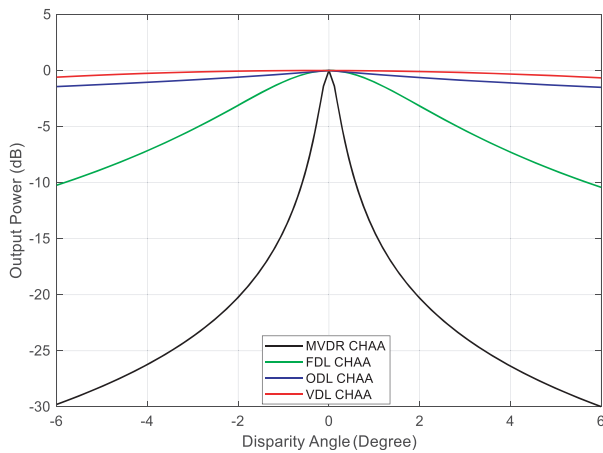


Figure 6. Output power vs. DOA error angle comparison of MVDR, FDL, ODL [16] and proposed VDL based robust CHAA beamformer.

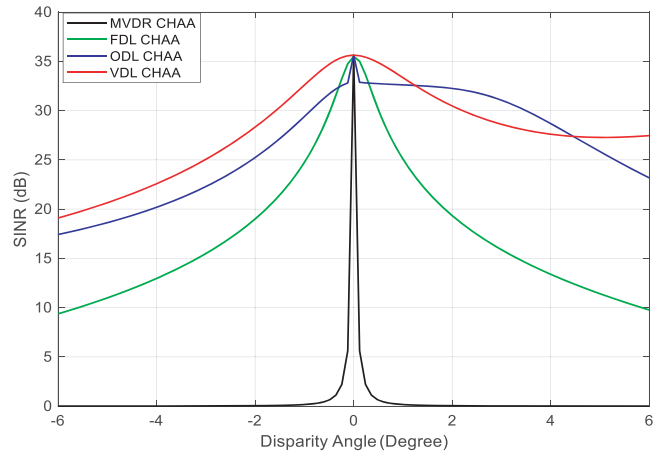


Figure 7. SINR vs. DOA error angle comparison of MVDR, FDL, ODL [16] and proposed VDL based CHAA.

compared with existing CCAA. So, the proposed CHAA provides better performance than the existing CCAA [7].

Figure 5 presents the power pattern comparison of MVDR, FDL, ODL [16] and VDL based robust CHAA with 2° DOA error. The assumed steering angle is 25°, and SOI incoming direction is 27°. Two interference signals have been considered at -60° and 70°. In this figure, MVDR based CHAA creates null at 27° as MVDR based beamformer considers any signal as interference except the signal in the beam steering direction. FDL and ODL based CHAA accept the SOI in the presence of DOA error by broadening its beam, but ODL based CHAA is more robust than FDL based CHAA. The proposed VDL based CHAA receives the SOI with higher power than FDL and ODL based CHAA. For several DOA angle errors, the power received by the CHAA utilizing different robust methods are listed in Table 1. For example, for 2° DOA error, the proposed VDL based CHAA delivers 88.37% and 78.56% higher output power than existing FDL and ODL [16] based CHAAs, respectively. So, the proposed VDL based CHAA is more robust than existing FDL and ODL [16] based CHAAs.

Figures 6 and 7 present the output power and SINR comparison of MVDR, FDL, ODL [16] and

Table 1. Output power of MVDR, FDL, ODL, [16] and proposed VDL based CHAA for several DOA angle error.

Beamforming Techniques	Output power values in dB for several DOA error angle				
	Without DOA error	1° DOA error	2° DOA error	3° DOA error	4° DOA error
MVDR	0	-13.2924	-24.94	-32.5873	-38.1919
FDL	0	-0.5612	-2.0846	-4.2064	-6.5913
ODL [16]	0	-0.6178	-1.1311	-1.5619	-1.9293
VDL [proposed]	0	-0.092	-0.2425	-0.4524	-0.7241

proposed VDL based CHAA with alteration of DOA error angle. In these figures, we can see that output power and SINR of MVDR based CHAA are reduced very much with a small increment of DOA error angle. FDL and ODL based CHAA provides higher power and SINR with the increment of disparity angle than MVDR based CHAA. The proposed VDL based CHAA provides the maximum power and higher SINR with the increment of disparity angle compared to other existing CHAAs [16].

Figure 8 shows the output SINR vs. SNR, and Fig. 9 shows the SINR vs. noise power of MVDR, FDL, ODL [16] and proposed VDL based CHAA. The presence of noise, interference, and DOA error has been considered in both figures. From Fig. 8, we perceive that the proposed CHAA utilizing VDL method delivers higher SINR than existing MVDR, FDL, and ODL [16] based CHAAs with the increase of SNR. From Fig. 9 it is ascertained that the proposed CHAA using VDL method delivers higher SINR in the presence of noise than existing MVDR, FDL, and ODL [16] based CHAAs.

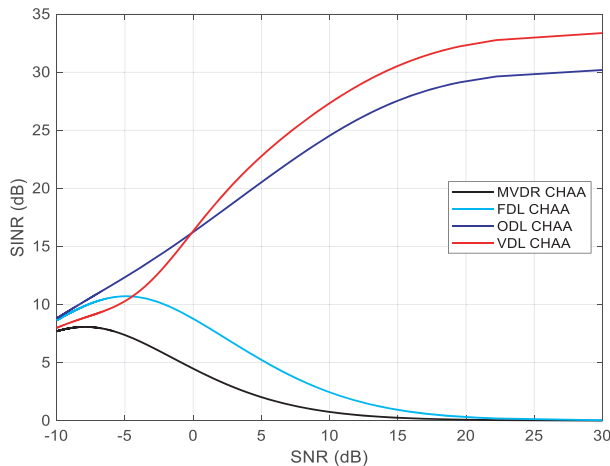


Figure 8. Output SINR variation with the alteration of input SNR of MVDR, FDL, ODL [16] and proposed VDL based robust CHAA in appearance of 1° DOA error.

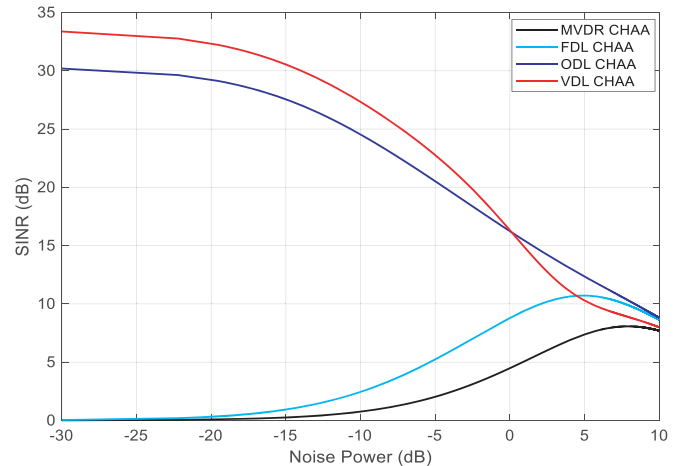


Figure 9. Output SINR variation with the alteration of noise power of MVDR, FDL, ODL [16] and proposed VDL based robust CHAA in appearance of 1° DOA error.

The selection of inter-element spacing is very significant. The impact of the alteration of this inter-element space on power pattern is shown in Fig. 10. In this figure, the power pattern curves are for the inter-element spaces of 0.25, 0.5, and 0.75 wavelength, respectively. We can see that when the space is less than 0.5 wavelength, the beamwidth of the main beam becomes very wide. When this space is larger than 0.5 wavelength, the beamwidth becomes narrow, but the side lobe level is increased, and more than one grating lobes are created. Hence, it is optimum to use the inter-element spacing equal to 0.5 wavelength.

Elements number of an array has impact on the power pattern of the array which is shown in Fig. 11

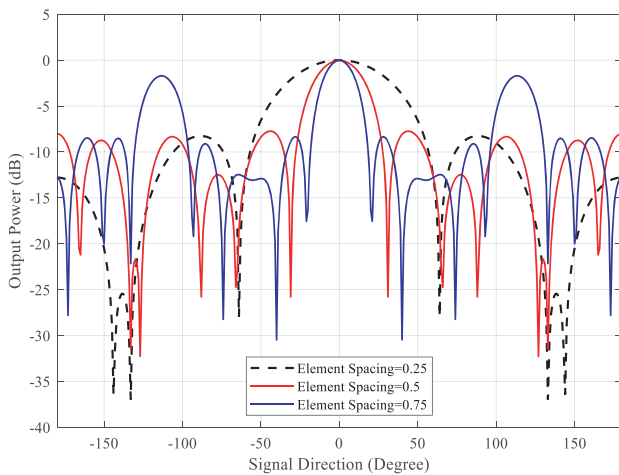


Figure 10. Impact of inter-element space variation on power pattern.

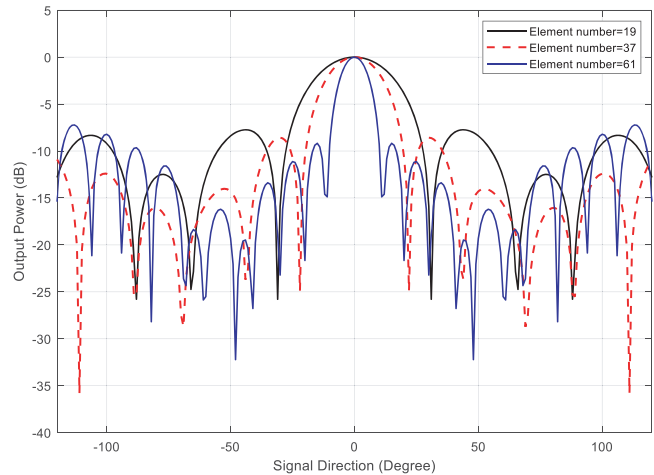
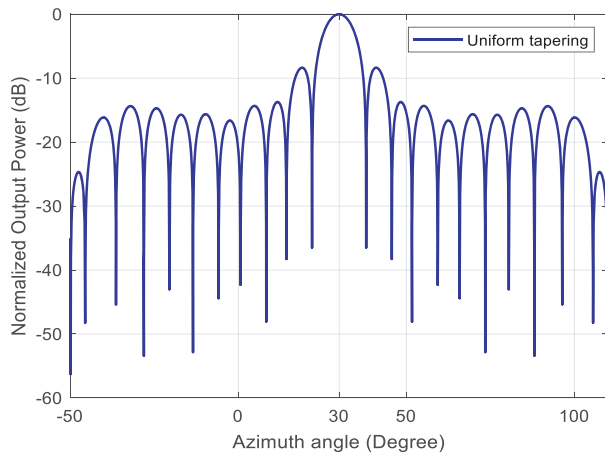
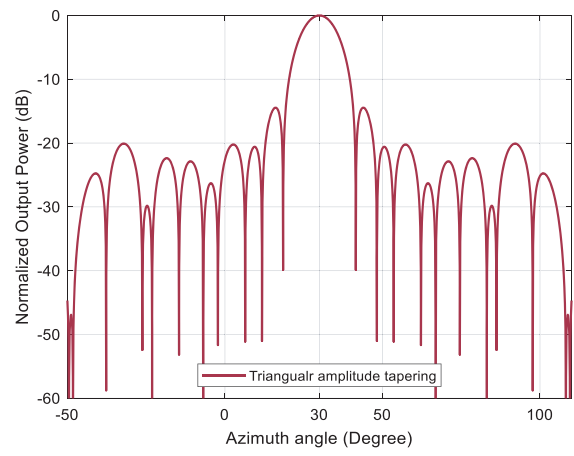


Figure 11. Output power for different number of antenna elements.

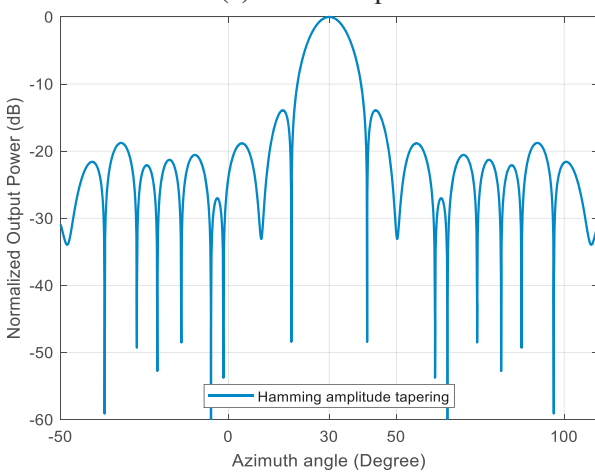
for CHAA. In this figure, there are three power pattern curves for 19, 37, and 61 antenna elements, respectively. From this figure, it is noticed that with the increment of number of antenna elements, the beamwidth of the main lobe becomes narrow, and side lobe power level is decreased.



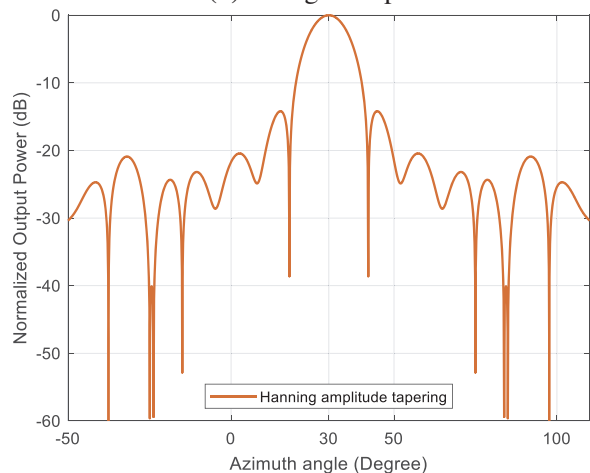
(a) Uniform tapered



(b) Triangular tapered



(c) Hamming tapered



(d) Hanning tapered

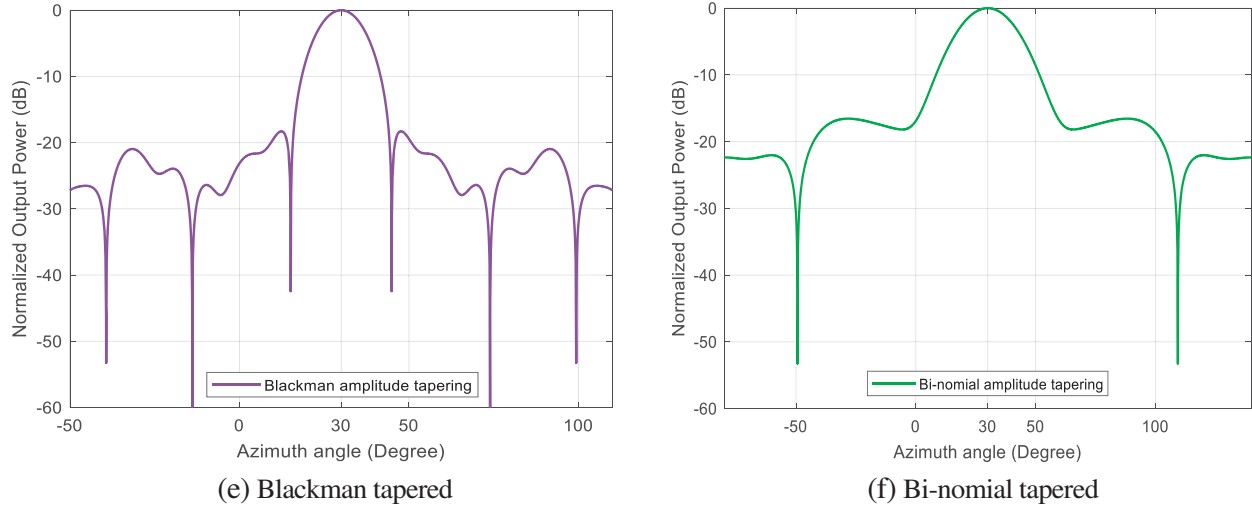


Figure 12. Typical radiation pattern of (a) uniformly fed, (b) triangular tapered, (c) Hamming tapered, (d) Hanning tapered, (e) Blackman tapered, (f) binomial tapered with 10-ring CHAA beamformer.

Figures 12(a)–(f) depict the typical normalized output power pattern of a centered element CHAA beamformer with 10 hexagonal rings by using modified Uniformly feeding window, Triangular window, Hamming window, Hanning window, Blackman window, and Binomial window respectively which are described in Section 4 and in [28]. From those figures, it is noticed that the SLL is decreased due to the use of various tapering windows in comparison to the uniformly tapered CHAA system. Binomial window technique results in minimum possible SLL and maximum beamwidth compared with other tapered schemes. Binomial window provides lower SLL than other window functions.

Figure 13 represents the SLL comparison of Uniformly feeding window, Triangular window, Hamming window, Hanning window, Blackman window, and Binomial window based beamformers with the alteration of number of hexagonal rings in the CHAA structure. From these figures we observe that in general SLL is reduced for all windows with the increment of number of hexagonal rings in the hexagonal structure except the uniformly feed window. Uniform feed window produces maximum SLL while the binomial window produces minimum possible SLL.

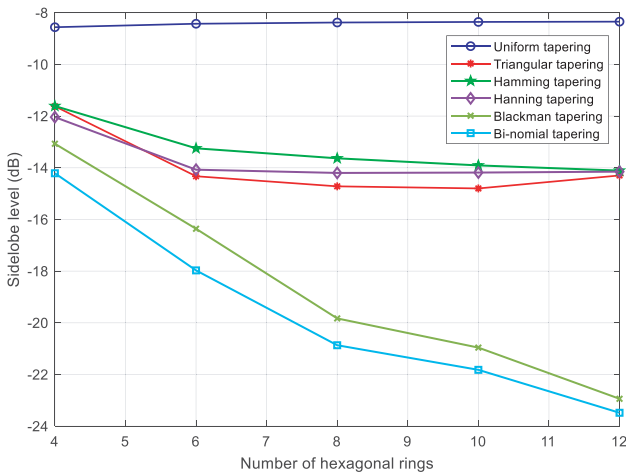


Figure 13. SLL comparison of different tapered beamformers with the alteration of number of hexagonal rings.

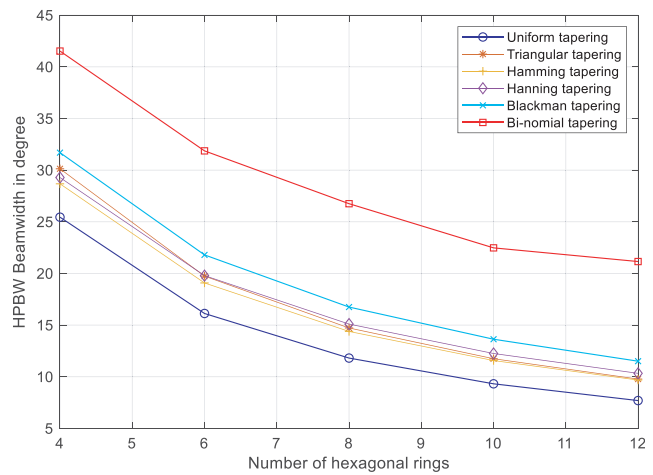


Figure 14. Half-power beamwidth comparison of different tapered beamformers with the alteration of number of hexagonal rings.

Figure 14 shows the HPBW comparison of the main lobe for different tapering window schemes as a function of number of rings in the hexagonal array. From this figure it is noticed that HPBW decreases with the increment of number of hexagonal rings in the array. The binomial window produces the highest beamwidth while uniform feeding window yields the lowest beamwidth.

From Figs. 13 and 14 considering SLL and HPBW, we can ascertain that Blackman tapering window is best suited for the proposed CHAA for the trade-off between HPBW and SLL. Fig. 15 shows the normalized power pattern of FDL, ODL, and VDL based robust CHAA using Blackman tapering window where SLL is significantly reduced. In this figure, estimated SOI direction, actual SOI direction, and an interference direction are 30° , 32° , and -20° , respectively. So, the proposed tapered robust concentric hexagonal antenna array provides better interference rejection capability, higher directivity, lower SLL, and robustness in the presence of DOA error.

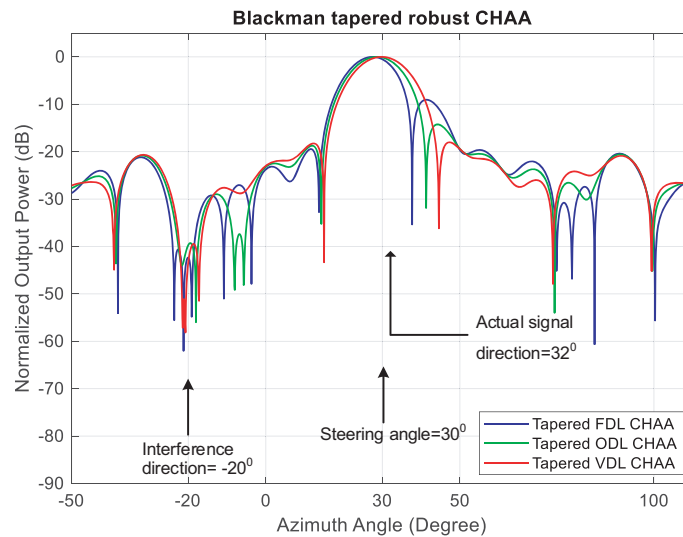


Figure 15. Normalized power pattern of Blackman window tapered FDL, ODL and VDL based CHAA.

6. CONCLUSION

A robust CHAA beamformer exploiting VDL technique has been addressed in this paper. The CHAA beamformer provides 25.54% narrow HPBW and lower SLL than existing CCAAs [7]. The MVDR based CHAA is able to detect and reject interference, but the performance of this beamformer is deteriorated when DOA angle error occurs. In the presence of DOA angle error, this paper proposes a VDL robust technique for CHAA beamformer. From the result analysis, we observe that the proposed VDL based CHAA delivers 88.37% and 78.56% higher output power for 2° DOA angle error than existing FDL and ODL [16] based CHAAs, respectively. Various modified tapering window functions have been proposed to minimize the SLL of the CHAA beamformer among which Blackman tapering window is best suited for the proposed CHAA. The practical implementation of CHAA in any application with an antenna prototype is a future scope of this paper.

REFERENCES

1. Viani, F., et al., "Exploitation of parasitic smart antennas in wireless sensor networks," *Journal of Electromagnetic Waves and Applications*, Vol. 24, No. 7, 993–1003, 2010.
2. Godara, L. C., *Smart antennas*, CRC press, 2004.
3. Fernandez-Olvera, A. D. J., D. Melazzi, and V. Lancellotti, "Beam-forming and beam-steering capabilities of a reconfigurable plasma antenna array," *Progress In Electromagnetics Research C*, Vol. 65, 11–22, 2016.

4. Khan, M. Z. U., et al., "Robust LCMV beamformer for direction of arrival mismatch without beam broadening," *Wireless Personal Communications*, Vol. 104, No. 1, 21–36, 2019.
5. Pappula, L. and D. Ghosh, "Linear antenna array synthesis using cat swarm optimization," *AEU-International Journal of Electronics and Communications*, Vol. 68, No. 6, 540–549, 2014.
6. Ram, Gopi, et al., "Cat swarm optimization as applied to time-modulated concentric circular antenna array: Analysis and comparison with other stochastic optimization methods," *IEEE Transactions on Antennas and Propagation*, Vol. 63, No. 9, 4180–4183, 2015.
7. Reza, M. F. and M. S. Hossain, "Robust concentric circular antenna array with variable loading technique in the presence of look direction disparity," *Progress In Electromagnetics Research M*, Vol. 57, 35–43, 2017.
8. Ganz, M. W., R. L. Moses, and S. L. Wilson, "Convergence of the SMI and the diagonally loaded SMI algorithms with weak interference," *IEEE Transactions on Antennas and Propagation*, Vol. 38, No. 3, 394–399, 1990.
9. Gan, L. and Z. Yi, "Automatic computation of diagonal loading factor for robust adaptive beamforming based on Gaussian distribution," *AEU-International Journal of Electronics and Communications*, Vol. 67, No. 7, 570–573, 2013.
10. Li, J., P. Stoica, and Z. Wang, "On robust Capon beamforming and diagonal loading," *IEEE Transactions on Signal Processing*, Vol. 51, No. 7, 1702–1715, 2003.
11. Hossain, M. S., L. C. Godara, and M. R. Islam, "Efficient robust broadband beamforming algorithms using variable loading," *IEEE Latin America Transactions*, Vol. 10, No. 3, 1697–1702, 2012.
12. Li, J., P. Stoica, and Z. Wang, "On robust Capon beamforming and diagonal loading," *IEEE Transactions on Signal Processing*, Vol. 51, No. 7, 1702–1715, 2003.
13. Wang, W., R. Wu, and J. Liang, "A novel diagonal loading method for robust adaptive beamforming," *Progress In Electromagnetics Research C*, Vol. 18, 245–255, 2011.
14. Reza, M. F. and M. S. Hossain, "Performance investigation of robust concentric circular antenna array beamformer in the presence of look direction disparity," *AEU-International Journal of Electronics and Communications*, Vol. 82, 52–57, 2017.
15. Song, A., et al., "Widely linear generalized sidelobe canceling beamforming with variable diagonal loading," *AEU-International Journal of Electronics and Communications*, Vol. 76, 77–85, 2017.
16. Ali, M. Y., M. S. Hossain, and M. F. Reza, "Robust hexagonal antenna array with optimal diagonal loading in the presence of steering angle disparity," *IEEE 4th International Conference on Electrical Information and Communication Technology (EICT)*, 1–5, 2019.
17. Mahmoud, K. R., M. El-Adawy, S. M. M. Ibrahim, R. Bansal, and S. H. Zainud-Deen, "A comparison between circular and hexagonal array geometries for smart antenna systems using particle swarm optimization algorithm," *Progress In Electromagnetics Research*, Vol. 72, 75–90, 2007.
18. Bera, R., et al., "Comparative study of circular and hexagonal antenna array synthesis using improved particle swarm optimization," *Procedia Comp. Sc. (Science Direct)*, Vol. 45, 651–660, 2015.
19. Liu, C., Y. Liu, Y. Zhao, and D. Hu, "Robust adaptive wideband beamforming using probability-constrained optimization," *Progress In Electromagnetics Research C*, Vol. 52, 163–172, 2014.
20. Huang, Y., M. Zhou, and S. A. Vorobyov, "New designs on MVDR robust adaptive beamforming based on optimal steering vector estimation," *IEEE Transactions on Signal Processing*, Vol. 67, No. 14, 3624–3638, 2019.
21. Qin, L., M. Wu, and Z. Dong, "Robust adaptive beamforming using multi-snapshot direct data domain approach," *AEU-International Journal of Electronics and Communications*, Vol. 75, 124–129, 2017.
22. Gu, Y., et al., "Robust adaptive beamforming based on interference covariance matrix sparse reconstruction," *Signal Processing*, Vol. 96, 375–381, 2014.

23. Shen, F., F. Chen, and J. Song, "Robust adaptive beamforming based on steering vector estimation and covariance matrix reconstruction," *IEEE Communications Letters*, Vol. 19, No. 9, 1636–1639, 2015.
24. Huang, L., et al., "Robust adaptive beamforming with a novel interference-plus-noise covariance matrix reconstruction method," *IEEE Transactions on Signal Processing*, Vol. 63, No. 7, 1643–1650, 2015.
25. Mandal, D., S. P. Ghoshal, and A. K. Bhattacharjee, "Design of concentric circular antenna array with central element feeding using particle swarm optimization with constriction factor and inertia weight approach and evolutionary programming technique," *Journal of Infrared, Millimeter, and Terahertz Waves*, Vol. 31, No. 6, 667–680, 2010.
26. Robinson, J. and Y. Rahmat-Samii, "Particle swarm optimization in electromagnetics," *IEEE Transactions on Antennas and Propagation*, Vol. 52, No. 2, 397–407, 2004.
27. Reza, M., M. Hossain, and M. Rashid, "Robust centered element concentric circular antenna array with low side lobe using variable loading and tapering windows in the presence of array imperfections," *International Journal of Antennas and Propagation*, 1–10, 2017.
28. Nofal, M., S. Aljahdali, and Y. Albagory, "Tapered beamforming for concentric ring arrays," *AEU-International Journal of Electronics and Communications*, Vol. 67, No. 1, 58–63, 2013.
29. Dessouky, M., H. Sharshar, and Y. Albagory, "A novel tapered beamforming window for uniform concentric circular arrays," *Journal of Electromagnetic Waves and Applications*, Vol. 20, No. 14, 2077–2089, 2006.
30. Donelli, M. and P. Febvre, "An inexpensive reconfigurable planar array for Wi-Fi applications," *Progress In Electromagnetics Research C*, Vol. 28, 71–81, 2012.
31. Wang, Y.-F., et al., "Wideband circularly polarized magneto-electric dipole 1×2 antenna array for millimeter-wave applications," *IEEE Access*, Vol. 8, 27516–27523, 2020.
32. Donelli, M., T. Moriyama, and M. Manekiya, "A compact switched-beam planar antenna array for wireless sensors operating at Wi-Fi band," *Progress In Electromagnetics Research C*, Vol. 83, 137–145, 2018.
33. Yuri, N. and P. Ilia, "Probability of false peaks occurring via circular and concentric antenna arrays DOA estimation," *2016 39th International Conference on Telecommunications and Signal Processing (TSP)*, 178–181, 2016.
34. Sarkar, P. K. and M. F. Reza, "Performance analysis of uniform concentric circular antenna array beamformer using different DOA estimation technique," *2018 4th International Conference on Electrical Engineering and Information & Communication Technology (iCEEiCT)*, 320–324, 2018.
35. Diniz, P. S., E. A. Da Silva, and S. L. Netto, *Digital Signal Processing: System Analysis and Design*, Cambridge University Press, 2010.